

# Identification of regions of fastest mixing in a system of point vortices

Prabhu Ramachandran and S. C. Rajan<sup>\*,†</sup>

*Department of Aerospace Engineering, Indian Institute of Technology Madras, Chennai, India*

## SUMMARY

This paper describes a numerical method for efficiently identifying the regions of fastest mixing of a passive dye in a flow due to a system of point vortices. Results obtained from computations are presented for systems of three and four point vortices, both in the unbounded domain and inside a circular cylinder. The flow is two-dimensional and the fluid is incompressible. The regions where mixing is possible are found by studying the largest Lagrangian Lyapunov exponent distribution with respect to various initial positions of tracer particles. The regions of fastest mixing are then identified from the Lyapunov exponent distribution at small times. The results of the method are verified by quantifying the mixing by using a traditional box counting technique. The technique is then applied to several different initial configurations of vortices and some interesting results are obtained. Some numerical findings about the nature of the exponents computed are also discussed. Copyright © 2002 John Wiley & Sons, Ltd.

KEY WORDS: chaos; Lyapunov exponent; mixing; point vortices

## 1. INTRODUCTION

Understanding the phenomenon of mixing and the quantitative prediction of the rate of mixing is important and has a wide variety of applications in aerospace and chemical engineering. It is a well-known fact that efficient mixing of fluids is intimately connected with chaos [1]. Novikov [2] considered a system of three vortices as a model of two-dimensional turbulence and obtained an exact solution to the problem of interaction of three identical vortices. Aref [3] presented an innovative qualitative analysis for the motion of three vortices having arbitrary strengths. Aref and Pomphrey [4, 5] presented numerical evidence of chaos in four point vortex systems and also showed formally that the three-vortex problem was integrable and that the four-vortex problem is not. The recent work of Babiano *et al.* [6] is also concerned with chaos in point vortex systems. Their finding is that irrespective of the fact that the velocity field displays Eulerian chaos (it is to be noted here that such a velocity field implies that the vortex motion is chaotic) or not, near the eye of the vortices there is regular Lagrangian motion,

---

\*Correspondence to: S. C. Rajan, Department of Aerospace Engineering, Indian Institute of Technology Madras, Chennai 600 036, India.

†E-mail: rajan@aero.iitm.ernet.in

characterized by a null Lagrangian Lyapunov exponent. However, the issues of mixing are not addressed in these articles. The mixing induced by a pair of fixed blinking vortices was studied by Aref [7]. The blinking vortices are point vortices that are alternately turned on and off. This is similar to having two fixed rotating cylindrical stirrers that abruptly switch on and off. Aref identified different conditions for efficient mixing by placing blobs of tracer particles and studying their advection. However, questions regarding the regions of high and low mixing were not addressed. Franjone and Ottino [8] discuss the computational difficulties involved in numerically tracking the evolution of material lines in order to study mixing. Aref [9] provides an excellent review of the topic of vortex motion in two-dimensional flows. The question of efficient identification of regions of mixing is not addressed in these works.

This paper is concerned with mixing in point vortex systems. A simple technique is presented to identify the regions of fastest mixing in such systems. Regions of mixing are identified by numerically calculating the distribution of the largest Lagrangian Lyapunov exponent of the flow with respect to the initial position of tracer particles for a given initial configuration of the point vortices. Subsequently, the regions of fastest mixing are identified by studying the exponent distribution at small times. Such a scheme is both easy to implement and more efficient than the traditional box counting schemes and a comparison between the two is also presented in this work. It is to be noted that it would be extremely hard to carry out an analytical study as performed by Aref for the motion of three vortices. A linear stability analysis is not of much use for such systems as one cannot find fixed points in the flow for all times. Studying this system numerically, in which the particle paths are governed by ordinary differential equations (ODEs), is much easier. The method employed to identify the regions of most efficient mixing in the flow is first described in detail with the help of a three vortex problem, having a specific initial configuration of the vortices. The method is then applied to a few different initial configurations of three and four vortices and some interesting results are obtained. Henceforth the term 'Lyapunov exponent' will refer to the largest Lagrangian Lyapunov exponent unless otherwise mentioned. From the computations it is found that when the vortices are constrained to move in a circular orbit, there are no regions in the flow where mixing is possible, and the Lyapunov exponents are all zero. When this vortex configuration is perturbed, regions of chaotic tracer motion gradually appear, having a positive Lyapunov exponent. These regions are interspersed with regular regions having a null Lyapunov exponent. As earlier reported by Babiano *et al.* [6], there is always a regular region surrounding each of the point vortices. Apart from these there are other regular regions that are identified and as the vortex configuration is further perturbed, more chaotic regions appear and the regular regions that are not near the vortices slowly reduce in size, until finally there are no such regular regions. This is true for motion of the point vortices inside a circular cylinder as well.

It is also observed that when the vortex motion is regular, for all the tracer particles located at various initial locations, the Lyapunov exponents converge to one particular value. Hence it seems that for integrable vortex motion having a given initial configuration of vortices, the Lyapunov exponent for all the chaotic regions is the same. This behaviour is not seen for a chaotic four-vortex problem in an unbounded domain, and for such a case it is found that for the various tracer particles, the Lyapunov exponents do not converge sharply and their behaviour in time is not similar. However, if one considers the chaotic vortex motion inside a circular cylinder the Lyapunov exponents again converge to a single value. This behaviour is noticed even when more refined calculations are made. The purpose of the paper

is the demonstration of the present technique and we merely wish to mention that great care has to be taken while studying the accurate evolution of Lyapunov exponents in unbounded chaotic vortex flows. The method of identifying the highest mixing regions is verified with the traditional box counting technique. The present technique is shown to be far more efficient in terms of both time taken and memory requirements than the box counting method.

## 2. MATHEMATICAL FORMULATION

The equation of motion for a fluid particle in an Eulerian velocity field  $\vec{u}(\vec{x}, t)$  is given by

$$\frac{d\vec{x}}{dt} = \vec{u} \quad (1)$$

For a given initial location of the particle  $\vec{x}(0)$ , the above equation is integrated to find  $\vec{x}(t)$ . If the system is two-dimensional and incompressible (i.e.  $\nabla \cdot \vec{u} = 0$ ) then Equation (1) assumes a Hamiltonian form with  $\vec{x} = (x, y)$  and  $\vec{u} = (u, v)$ . The Hamiltonian is denoted as  $\psi$  and is the same as the streamfunction for the flow. Then the equations describing the motion of any fluid particle in the flow are given by

$$\begin{aligned} \frac{dx}{dt} &= u = \frac{\partial \psi}{\partial y} \\ \frac{dy}{dt} &= v = -\frac{\partial \psi}{\partial x} \end{aligned} \quad (2)$$

Consider the motion of passively advected fluid particles in a flow generated by  $N$  point vortices in an infinite domain. If the vortices have strengths  $\Gamma_i$  and positions given by  $(x_i(t), y_i(t))$ , for  $i = 1, 2, \dots, N$ , then the system can be considered as Hamiltonian, governed by the following equations:

$$\begin{aligned} \Gamma_i \frac{dx_i}{dt} &= \frac{\partial \psi}{\partial y_i} \\ \Gamma_i \frac{dy_i}{dt} &= -\frac{\partial \psi}{\partial x_i} \end{aligned} \quad (3)$$

where  $\psi$  is the Hamiltonian given by

$$\psi = -\frac{1}{4\pi} \sum_{i \neq j; i, j=1}^N \Gamma_i \Gamma_j \ln |r_{ij}|$$

and  $r_{ij}^2 = (x_i - x_j)^2 + (y_i - y_j)^2$ .

The trajectory of the point vortices can be obtained using Equation (3). There are four invariants for the vortex motion as given by Aref [9]. They are the Hamiltonian, the first moments and the second moment of the vortex strengths and are given below, respectively

$$\psi = -\frac{1}{4\pi} \sum_{i \neq j; i, j=1}^N \Gamma_i \Gamma_j \ln |r_{ij}|$$

$$P = \sum_{i=1}^N \Gamma_i x_i$$

$$Q = \sum_{i=1}^N \Gamma_i y_i$$

and

$$I = \sum_{i=1}^N \Gamma_i (x_i^2 + y_i^2)$$

Using these conserved quantities the algorithm being used for the numerical integration can be checked for accuracy. This has been performed by Prabhu [10] for the specific cases of a three-vortex problem and a chaotic four-vortex problem.

The path  $[x(t), y(t)]$  of an arbitrary fluid particle in the flow is governed by the following equations, where  $(x_i(t), y_i(t))$  are the co-ordinates of the position of the vortices:

$$\begin{aligned} \frac{dx}{dt} = u &= - \sum_{i=1}^N \frac{\Gamma_i}{2\pi} \frac{(y - y_i)}{(x - x_i)^2 + (y - y_i)^2} \\ \frac{dy}{dt} = v &= \sum_{i=1}^N \frac{\Gamma_i}{2\pi} \frac{(x - x_i)}{(x - x_i)^2 + (y - y_i)^2} \end{aligned} \quad (4)$$

Hence, for a given initial configuration of vortices in an unbounded domain and initial position of a fluid particle, its path can be found by numerically integrating Equations (3) and (4).

To compute the motion of particles inside a cylinder we merely use the corresponding image vortices and compute the flow in a similar manner to the unbounded domain case. If the position of a point vortex is given by the complex number  $z$  and the cylinder is of radius  $R$ , then it is well known that the image vortex to be considered is at  $R^2/\bar{z}$ , where  $\bar{z}$  is the complex conjugate of  $z$  and that its strength is the opposite of the strength of the actual point vortex.

It is known [9] that for vortex motion in an unbounded domain that if  $N > 2$ , the particle path can be chaotic even if the vortex motion is regular, and for the vortex motion to be chaotic at least four vortices are necessary. For motion inside a circular cylinder, if  $N > 1$  then the particle path can be chaotic, and for the vortex motion to be chaotic at least three vortices are needed. The algorithm used to integrate the equations is an adaptive step-size Runge–Kutta Cash–Karp algorithm as given by Press *et al.* [11], which is fourth-order accurate (error =  $O(\delta t^5)$ ). The computations require an error condition to be satisfied and this error parameter is called ‘eps’. The algorithm adjusts its time step such that the error introduced per step is less than eps.

### 3. COMPUTATION OF THE LARGEST LYAPUNOV EXPONENT

In order to quantify the degree of chaoticity of a system, the largest Lyapunov exponent of the flow is to be determined. Since the present work is concerned with mixing of a passive dye, only the largest Lagrangian Lyapunov exponent is to be computed. This exponent measures the average rate of exponential separation of two initially nearby orbits. The *ghost particle*

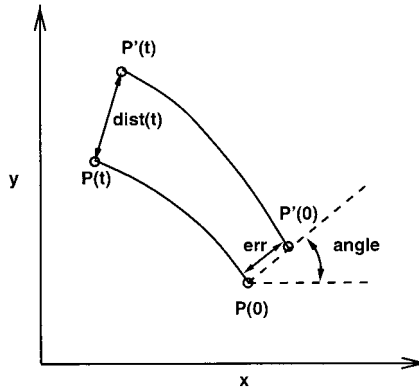


Figure 1. Illustration of the various quantities involved in the computation of the largest Lagrangian Lyapunov exponent, for the ghost particle technique.

technique as given in Peitgens *et al.* [12] is employed here. The velocity induced at any point in the flow field is given by Equations (4). Using Equations (3) and (4), the path of any fluid particle in the flow is computed. To calculate the Lyapunov exponent, a particle  $P$  and its ‘ghost’ at  $P'$  are considered, as in Figure 1. The distance between them at any time is given by  $\text{dist}(t)$  and the angle between the line joining  $P$  and  $P'$  and the  $x$ -axis initially is called ‘angle’. The Lagrangian Lyapunov exponent,  $\lambda_L$ , is then given by,

$$\lambda_L = \lim_{t \rightarrow \infty} \lim_{\text{dist}(0) \rightarrow 0} \frac{1}{t} \ln \left| \frac{\text{dist}(t)}{\text{dist}(0)} \right| \tag{5}$$

which gives an average exponential rate of separation of the paths of the two particles. If the orbit through  $P$  is chaotic then the value of  $\text{dist}(t)$  will grow exponentially and this will result in computational overflows and other errors. In order to circumvent this, a renormalization procedure is performed and  $\lambda_L$  is given by

$$\lambda_L = \lim_{t \rightarrow \infty} \lim_{\text{err} \rightarrow 0} \frac{1}{t} \sum_i \ln \left| \frac{\text{dist}(t_i)}{\text{err}} \right| \tag{6}$$

where  $\text{dist}(t_i)$  is the instantaneous distance between the two particles at time  $t_i$  and ‘err’ is the distance to which the particles are renormalized at time  $t_i$ . The two different types of curves for  $\lambda_L$  with time are shown in Figure 2. This figure is for an initial configuration of three vortices as described in the next section (case A). As can be seen from the figure, the orbits behave in two distinct ways. One is chaotic and has a Lyapunov exponent that tends to a positive limiting value. The other is a regular orbit that has a Lyapunov exponent that rapidly falls to zero. The Lyapunov exponent is, in general, a function of the initial position. In this work the relation between the exponent and the initial position is explored.

The method described above for computing the largest Lyapunov exponent depends on four parameters, which are  $\text{eps}$ ,  $\text{err}$ ,  $\text{angle}$  and  $t_{\text{max}}$ , the maximum time of computation. A computer program is developed that can calculate the largest Lagrangian Lyapunov exponent for a grid of initial positions of tracer particles by using the procedure described above for a general  $N$  point vortex problem. To compute the exponent efficiently, the above-mentioned parameters

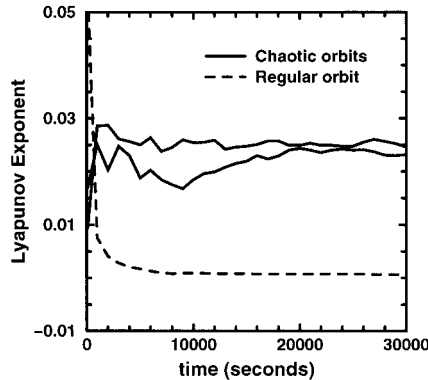


Figure 2. Illustration of the two different kinds of behaviour of the Lyapunov exponent in time.

must be chosen carefully. This is done by considering a set of initial points and finding the exponent at each of these points for various values of the above parameters. The details of the computations are given by Prabhu [10], where the parameter  $\text{err}$  is chosen such that it is about an order of magnitude larger than  $\text{eps}$ . It is found that the suitable values to be chosen are  $\text{eps} = 5 \times 10^{-7}$ ,  $\text{err} = 5 \times 10^{-6}$ . The angles are chosen randomly, i.e. the ghost particles are initially located at some random angle with respect to the particle being traced. Due to computational constraints, the upper limit of  $t_{\text{max}}$  is chosen as 30 000 s.

#### 4. COMPUTATIONS FOR A GRID OF INITIAL POINTS

The method is illustrated for the case of three point vortices initially at  $(x_1, y_1) = (1, 0)$ ;  $(x_2, y_2) = (-1, 0)$ ;  $(x_3, y_3) = (0, 1)$ . The strength  $\Gamma$  of each vortex is 1.0. This configuration is called case A.

For this case a grid of tracer points with an equal interval spacing of  $1/6$  units in  $x$  and  $y$  is taken. The Lyapunov exponents for the tracer orbits starting from the points on the grid are computed for a  $t_{\text{max}}$  of 30 000 s and is given in Figure 3. The figure is a contour plot of the Lyapunov exponent for various initial conditions of a fluid particle. For clarity only the significant contours are plotted. The figure shows the regions where there is regular motion. All the regions inside the closed 0.005 contours excluding the outermost contour and the region outside the peripheral contour have regular motion (they have Lyapunov exponents tending to zero) and the orbits starting from these regions are non-chaotic. The regions in-between the peripheral contour and the regular regions have chaotic motion. As can be seen there are large regular regions surrounding the eyes of the vortices. This result agrees with that obtained by Babiano *et al.* [6], in which they find that for systems of three and four point vortices, regular motion is seen near the eye of the vortices and further away from these vortices the motion is chaotic. However, as can be seen in the figure, there are also other regions of regular motion identified here that are not near the eyes of the vortices.

Figure 4 is a histogram of the number of points having a Lyapunov exponent in a given exponent range. The plots are, respectively, for  $t_{\text{max}} = 10\,000$  and 30 000 s. As seen in both plots, the exponent is either zero or has some positive value, but the plot for 30 000 s clearly

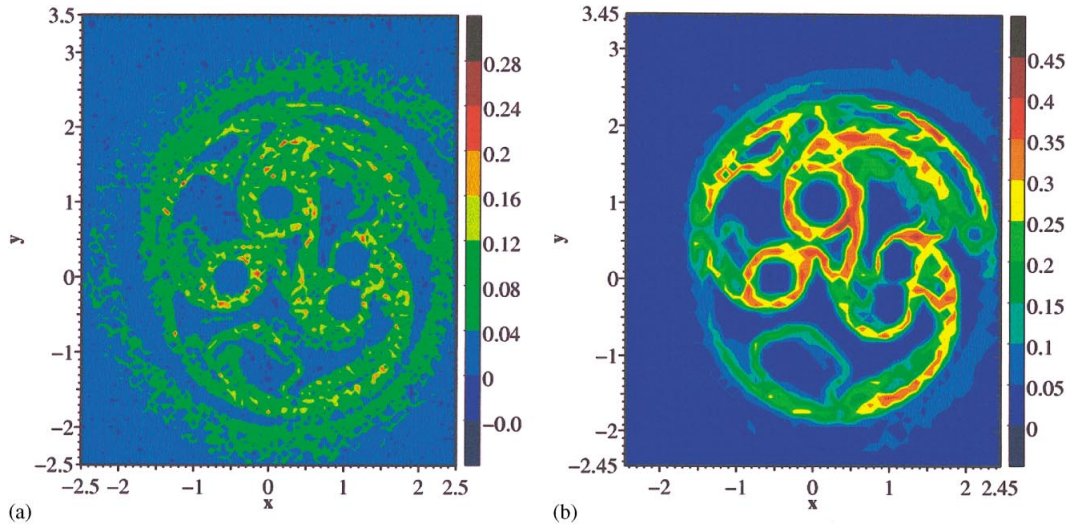


Plate 1. (a) Contour plot of the largest Lyapunov exponent for a set of four point vortices in the unbounded domain that move chaotically at a time of 50 s. (b) Contour plot of the occupied box fraction using the box counting scheme at various points in the flow at 50 s for the same configuration.

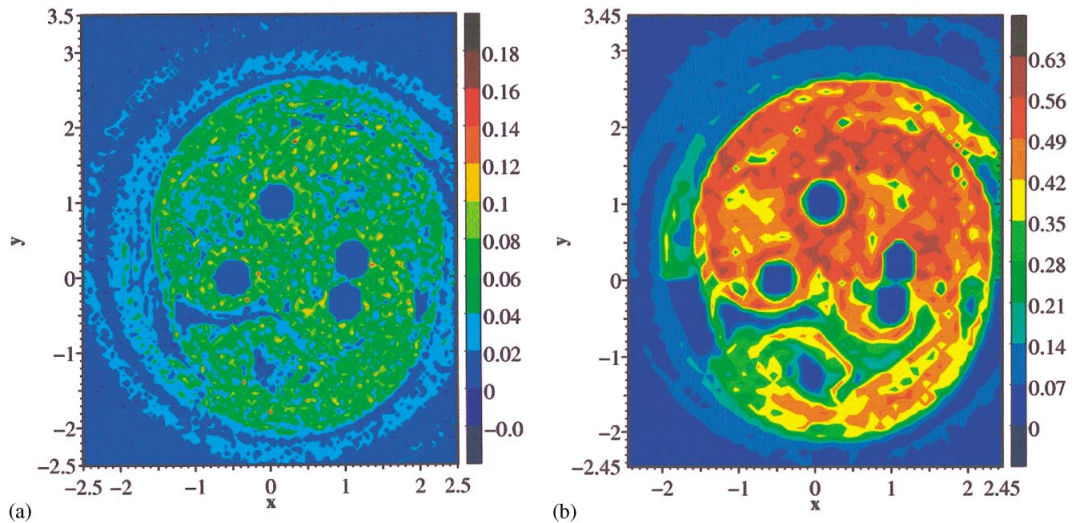


Plate 2. (a) and (b) Contour plots using the new technique and the box counting technique at 150 s for the same vortex configuration as in Plate 1.

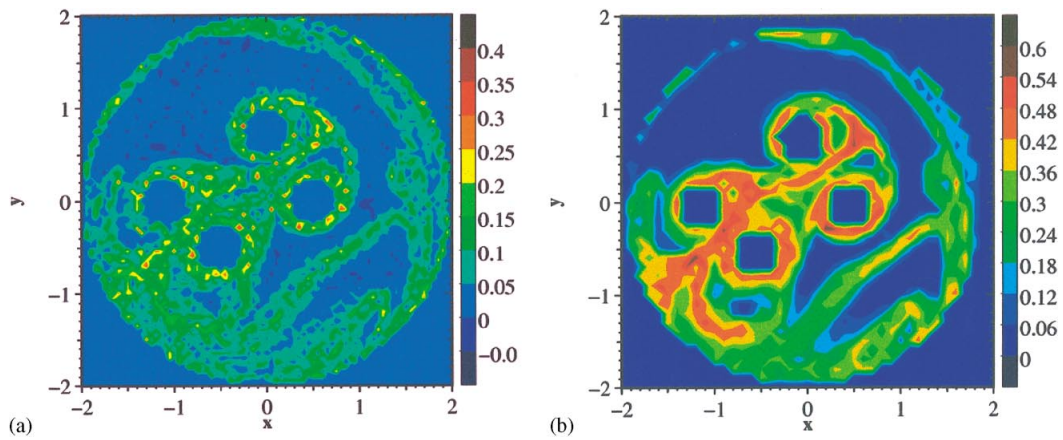


Plate 3. (a) Contour plot of the largest Lyapunov exponent for a set of four point vortices inside a circle that move chaotically at a time of 50 s. (b) Contour plot of the occupied box fraction at various points in the flow at 50 s for the same configuration.

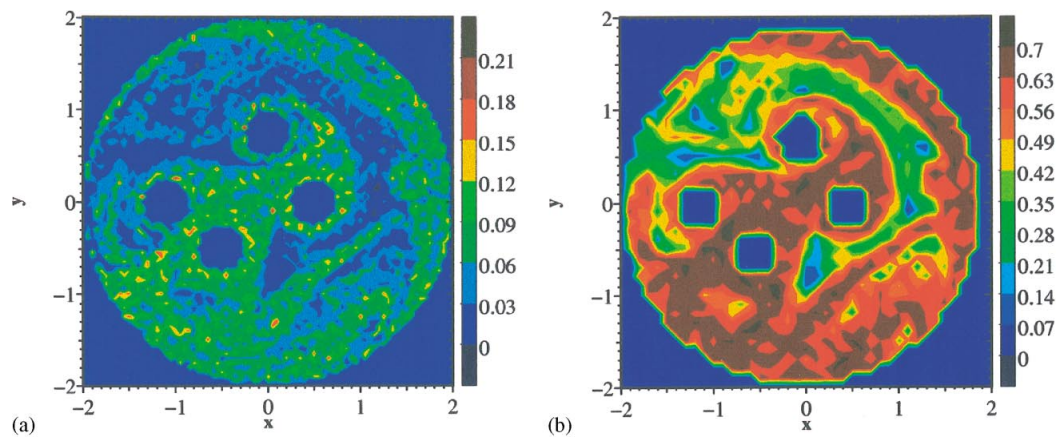


Plate 4. (a) and (b) Contour plots using the new technique and the box counting technique at 150 s for the same problem as in Plate 3.

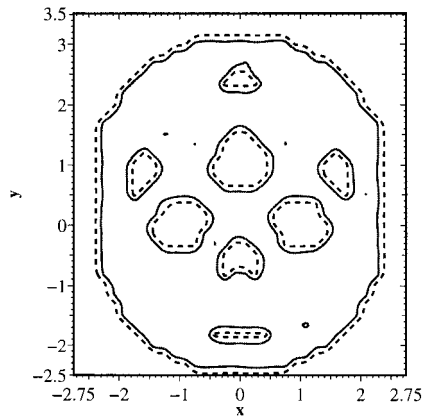


Figure 3. Contour plot of the Lyapunov exponents for different initial conditions of tracer particles. The initial vortex configuration is case A. The solid line is a 0.02 contour and the dashed line is a 0.005 contour.

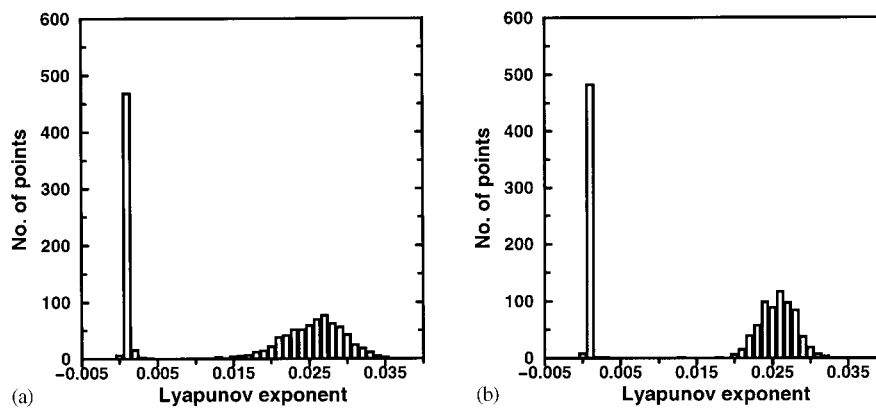


Figure 4. (a) and (b) Histograms for the Lyapunov exponents for various initial tracer locations at times of 10 000 and 30 000 s respectively.

has a narrower band than the former one. This seems to indicate that there are only two distinct values for the Lyapunov exponent, one zero and the other around 0.025.

In order to check whether the change from non-chaotic to chaotic motion near the eye of the vortex is gradual or abrupt, a finer grid of tracer particles is chosen near one of the vortices. The resulting contour plot is shown in Figure 5. It appears from the plot that the transition from a regular to a chaotic regime is abrupt.

From the calculated Lyapunov exponent distribution the regular and chaotic regions can be identified. As the next step, the Lyapunov exponent distribution is plotted for small times from which the regions of fastest mixing can be identified.

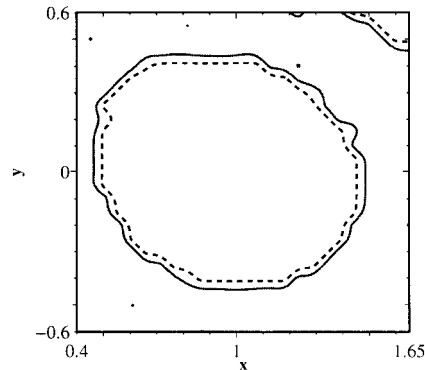


Figure 5. Contour plot for a finer grid of particles initially around the vortex located at (1,0) (case A). The solid line is a 0.02 contour and the dashed line is a 0.005 contour.

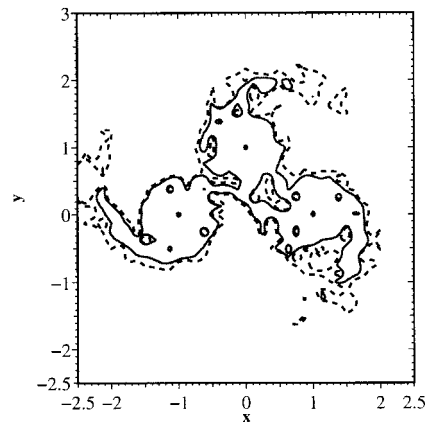


Figure 6. Contour plot of the small-time Lyapunov exponent distribution after a time of 10 s. (case A). The solid line is a 0.15 contour and the dashed line is a 0.1 contour.

## 5. LYAPUNOV EXPONENT DISTRIBUTION FOR SMALL TIMES

The very definition of the Lyapunov exponent implies that the computations be performed for as large a time as possible, but in order to understand the initial behaviour of the flow, the exponent distribution at small times is examined. This study of the exponent at small times indicates whether a blob placed in a given region stretches immediately or not. Thus, it has the potential of identifying the regions of fast and slow mixing. Based on the values obtained after 10 s, the Lyapunov exponent distribution is plotted in Figure 6 for the same initial vortex configuration as in case A and gives the small-time Lyapunov exponent distribution. The chosen values of  $\epsilon_{ps}$  and  $\epsilon_{rr}$  are same as in the previous case. There are many more contours that are obtained but for clarity only the significant ones are shown in the figure. The contours having a large Lyapunov exponent are the ones inside which there is a possibility of faster mixing. In the work done by Prabhu [10] it is found that the small-time Lyapunov

exponent distribution does not vary much when the angles of the ghost particles are changed. Hence, if a blob is placed in a region that is identified to be a chaotic one from the study of the exponent at large times, and that also has a large exponent value at small times, then it is expected that it will mix quickly. It may be mentioned that it is not sufficient to study the exponent distribution for a particular small time but for a number of small times (say, 10–50 s) in order to decide whether the region is truly a fast or slow mixing one. However, only the 10 s plot is presented here.

## 6. QUANTIFICATION OF MIXING

When a blob of ink mixes in a fluid it implies that the blob spreads throughout the fluid. One has to be able to quantify the rate of spreading of the blob. Computationally, the blob is made up of several points that are separated by very small distances. The quantification of mixing is carried out as follows. The domain of the flow is divided into several small boxes (the number of boxes is of the same order as the number of points in the blob). At any given time, the number of boxes in the domain that has a particle in it is counted. This number of occupied boxes is divided by the total number of boxes to get the fraction of occupied boxes in the domain. This fraction is plotted versus time and the slope of this curve indicates the rate of mixing. In Figures 7 and 8 a blob having initially a dimension of  $0.1 \times 0.1$  square units and having around 6500 particles in it, is studied for its mixing, based on this technique. In Figure 7, mixing in the regular regions is quantified. The blob is centred at  $(-1.7, 0.85)$  for an initial vortex configuration as mentioned earlier (case A). This is a regular region (refer to Figure 3) and is not close to the centre of any vortex. Similarly, a point at  $(0, 1.3)$  which is near the eye of one of the vortices, is chosen and the blob is centred there. The resulting curve is again shown in Figure 7. As can be seen, the mixing is very slow and the number of occupied boxes tends to a low constant value for both cases.

In Figure 8 one particular fast mixing region centred around the point  $(1.6, -0.45)$  is considered. The fast mixing region is identified from the small time Lyapunov exponent plot

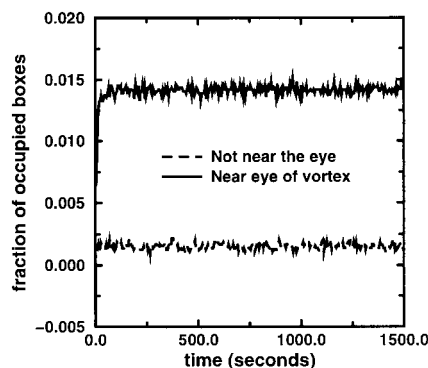


Figure 7. Quantitative plot of the mixing seen in the regular regions for case A. The solid line shows the mixing for a blob placed near the eye of a vortex and the dashed curve is for a blob placed in a regular region that is not near any of the vortices, surrounding which there are regions of chaotic motion.

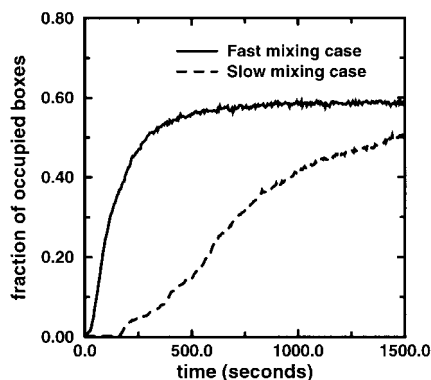


Figure 8. Mixing seen for fast and slow mixing regions in case A. The solid curve shows the mixing for a blob placed initially in a region having a large small-time Lyapunov exponent, whereas the dashed curve is for a blob placed in a region that has a small, small time Lyapunov exponent.

given in Figure 6. This figure also indicates that near the fast mixing region there is a region where the mixing is slower due to the fact that the small time exponent in the region is much smaller than that of the fast mixing regions. A slow mixing region is identified around the point (0.35, 1.65) and hence a blob is centred there. Figure 8 verifies the slower mixing region very well and the corresponding curve has a smaller slope than that for the blob placed in the fast mixing region. Hence the small-time Lyapunov exponent plot, together with the long-time Lyapunov exponent distribution, seems to be effective in identifying the regions of faster and slower mixing, and from them the regions of the fastest mixing can be identified. Figures 7 and 8 clearly confirm this observation.

The above simple verifications are not substantial enough to show with certainty that our scheme of identification is correct and hence an entire region of interest is considered and mixing is quantified by both the new technique and the box counting scheme and the results are compared. There are two arbitrary vortex configurations that are considered. The first is a set of four vortices having an initial configuration of  $\Gamma_1 = 0.7$ ,  $\Gamma_2 = 1.2$ ,  $\Gamma_3 = 0.9$ ,  $\Gamma_4 = 1.0$ ;  $(x_1, y_1) = (1.1, 0.23)$ ;  $(x_2, y_2) = (0.1, 1.0)$ ;  $(x_3, y_3) = (-5.0, 0.0)$ ;  $(x_4, y_4) = (1.0, -0.34)$  in the unbounded domain that have a chaotic path and the second set of four vortices inside a cylindrical vessel of radius 2 units having configuration of  $\Gamma_1 = 1$ ,  $\Gamma_2 = -1$ ,  $\Gamma_3 = 1$ ,  $\Gamma_4 = -1$ ;  $(x_1, y_1) = (-1.1, 0.0)$ ;  $(x_2, y_2) = (0.5, 0.0)$ ;  $(x_3, y_3) = (0.0, 0.0)$ ;  $(x_4, y_4) = (-0.5, -0.5)$  and having a chaotic path.

While quantifying the mixing using the box counting scheme, the domain of interest is divided into  $N$  small cells of size  $0.1 \times 0.1$ . Each of these cells contains 100 particles. For each of these cells the mixing is quantified using the box counting scheme. At each time interval the value of the fraction of occupied boxes due to each cell is contour plotted. In the new technique, the largest Lyapunov exponent is computed for a uniform grid of  $4N$  particles and then contour plotted at the required times. The results for the four-vortex problem in the unbounded domain at 50 s is plotted in Plate 1. Plate 1(a) shows the result with the new technique and Plate 1(b) shows the result for the box counting case. Similarly, the plot for the mixing at 150s is shown in Plate 2. It is to be noted that by this time a very large amount of mixing has taken place and the mixing is nearly complete. For the case of the vortices

inside a circular cylinder the plots at 50 s are shown in Plate 3 and the plots for 150 s are shown in Plate 4. As can be clearly seen from the plots, apart from the difference in the actual numerical values (and hence the colouring), which is only expected since one figure gives the Lyapunov exponent and the other gives the fraction of occupied boxes, that the agreement is excellent. All the significant features of importance, such as the relative regions of high and low mixing, are very clearly identifiable from the contour plot of the Lyapunov exponent and these match very well with the results obtained from the box counting technique.

One of the main advantages of the present technique is that it is much more efficient than the box counting method both in terms of time taken as well as memory resources used for the computation. This is clearly seen from the following discussion. For a small region of size  $0.1 \times 0.1$ , 100 particles were advected in the box counting scheme, whereas only four particles were considered for the Lyapunov exponents. To compute the exponent at these four points, eight particles are needed since the ghost particle technique is used. Hence this scheme is more efficient by a factor of 12.5 both in terms of time and memory and yet effective in identification of the regions of fastest mixing.

## 7. BEHAVIOUR OF THE BLOB IN TIME

The evolution in time of a blob of tracer particles placed in either a chaotic or a regular region for an initial vortex configuration as in case A is studied. When the blob is placed in a chaotic region it mixes in the fluid and does not visit the regions where the motion is regular. This is seen in Figure 9.

There are two types of regular behaviour that are observed. In the regular region near the eye of the vortex, the blob stretches rapidly but the stretching is localized, i.e. it stretches enormously but is confined in the vicinity of the vortex. This is seen in Figure 10. However, in the other regular regions that are not near the eyes of the vortices, the blob hardly stretches and it more or less retains its shape (Figure 11).

## 8. RESULTS FOR OTHER INITIAL CONFIGURATIONS OF VORTICES

### 8.1. Integrable vortex motion

In this section the method described above is applied to other initial configurations of three and four vortices that have integrable vortex motion.

To begin with, the case of three vortices initially placed at the vertices of an equilateral triangle of side 2 units is considered. The strength and position of the vortices are, respectively,  $\Gamma_1 = \Gamma_2 = \Gamma_3 = 1.0$ ;  $(x_1, y_1) = (-1, 0)$ ;  $(x_2, y_2) = (1, 0)$ ;  $(x_3, y_3) = (0, \sqrt{3})$ . This is called case B. For this case the vortices move on a circle centred at the centroid of the equilateral triangle. It is found that the exponent value is extremely small and that it decreases rapidly in time. This indicates that there is no positive Lyapunov exponent in such a flow and that there is no possibility of mixing.

The above initial configuration of vortices is slightly perturbed resulting in an initial configuration called case C and is given by  $\Gamma_1 = \Gamma_2 = \Gamma_3 = 1.0$ ;  $(x_1, y_1) = (-1, 0)$ ;  $(x_2, y_2) = (1, 0)$ ;  $(x_3, y_3) = (0, 1.6)$ . For this case the Lyapunov exponent distribution is given in Figure 12. As

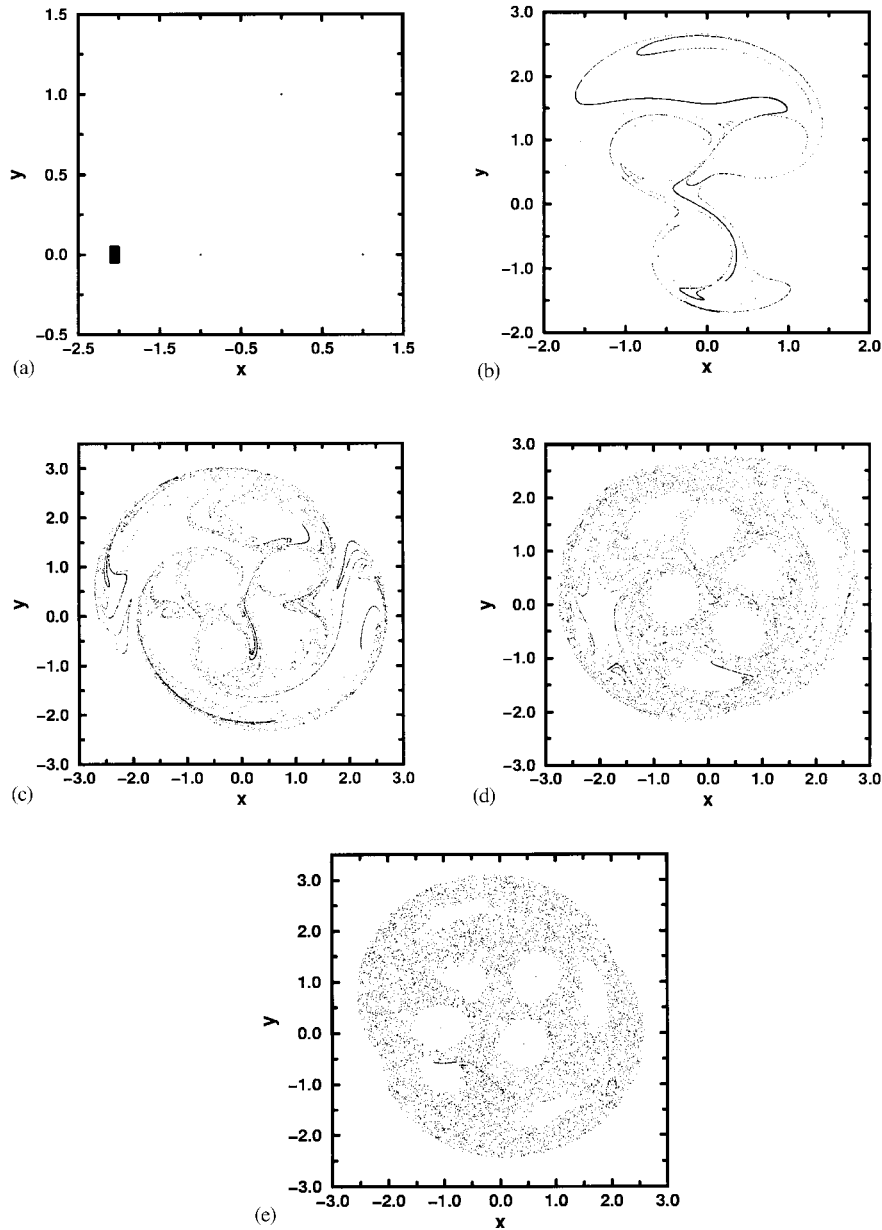


Figure 9. (a)–(e) show the evolution of a blob in time at 0, 50, 150, 300, 600 s respectively for case A. The blob is placed in a region which is identified as a chaotic and fast mixing one.

mentioned earlier, only the significant contours are presented. It can be clearly seen that there are large regions having a null Lyapunov exponent and small bands where it is positive. Hence it seems that, if the perturbation of the initial vortex positions is increased, larger regions of chaotic tracer motion may be seen.

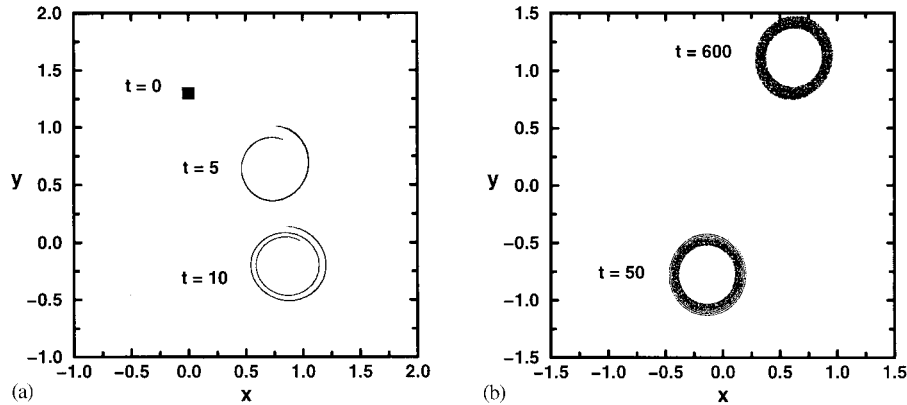


Figure 10. (a) and (b) show the development of a blob in time that is placed near the eye of a vortex (case A).

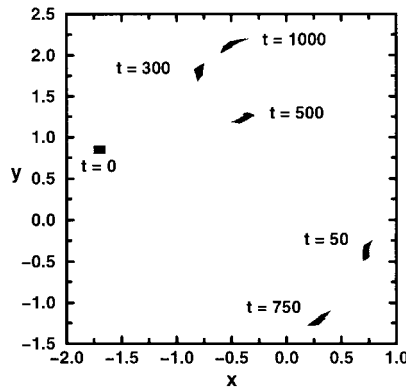


Figure 11. Plot showing the development of a blob placed in a regular region that is not near the vortices and is surrounded by regions of chaotic tracer motion (case A).

Earlier for case A, where three point vortices initially formed an isosceles triangle, it was seen that there were regular regions near the eyes of the vortices. Other regions of regular motion were also identified and were given in Figure 3. This configuration of vortices is significantly different from case B (vortices placed on an equilateral triangle), where the entire region has regular motion. Hence, from the results of cases A and C, it seems that as the circular motion of the vortices is slowly perturbed, the regular regions gradually break up into distinct regions having either regular or chaotic motion.

In order to check this, the configuration of the three vortices is made asymmetric by choosing the initial co-ordinates as  $(x_1, y_1) = (-1, 0)$ ;  $(x_2, y_2) = (1, 0)$ ;  $(x_3, y_3) = (0.5, 0.75)$  and choosing  $\Gamma_1 = \Gamma_2 = \Gamma_3 = 1.0$ . This is called case D and its Lyapunov exponent distribution is given in Figure 13. For this case it is clearly seen that there are about four regular regions apart from the ones near the eyes of the vortices but these are very small in size compared to those seen in Figure 3 (case A).

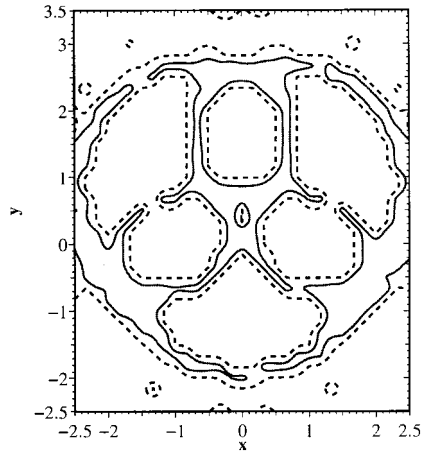


Figure 12. Contour plot of the Lyapunov exponent distribution for case C and for a  $t_{\max}$  of 20 000 s. The solid line is a contour of 0.01 and the dashed line is a 0.001 contour.

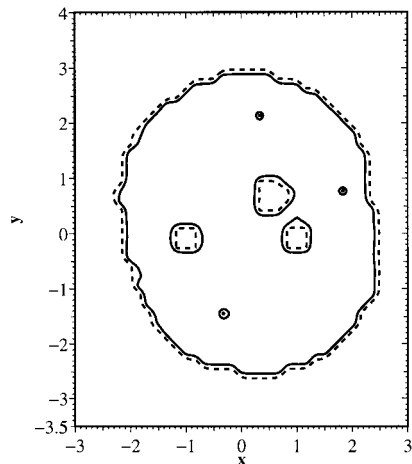


Figure 13. Contour plot of the Lyapunov exponent distribution for case D and for a  $t_{\max}$  of 20 000 s. The solid line is a contour of 0.018 and the dashed line is a 0.003 contour.

The initial configuration of case D is further altered by making it more asymmetric. The chosen initial configuration is  $\Gamma_1 = \Gamma_2 = \Gamma_3 = 1.0$ ;  $(x_1, y_1) = (-1, 0)$ ;  $(x_2, y_2) = (1, 0)$ ;  $(x_3, y_3) = (1, 1)$ . This case is called case E and the Lyapunov exponent distribution is given in Figure 14. It can be seen that there is only one regular region of motion apart from the ones near the eyes of the vortices and this also is very small. This indicates that in order to have large regions in the flow where the tracer motion is chaotic, the initial vortex configuration of case B must be altered significantly.

Three vortices on a line are considered next and this is called case F. The initial configuration of the vortices is  $\Gamma_1 = \Gamma_2 = \Gamma_3 = 1.0$ ;  $(x_1, y_1) = (-1, 0)$ ;  $(x_2, y_2) = (0, 0)$ ;  $(x_3, y_3) = (1, 0)$ .

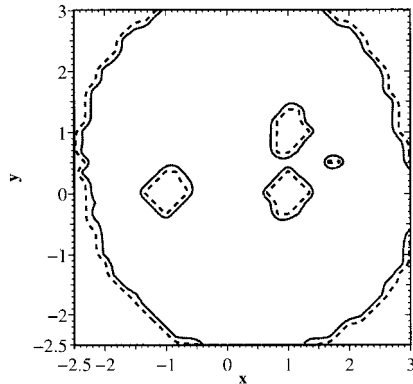


Figure 14. Contour plot of the Lyapunov exponent distribution for case E and for a  $t_{\max}$  of 20 000 s. The solid line is a contour of 0.015 and the dashed line is a 0.003 contour.

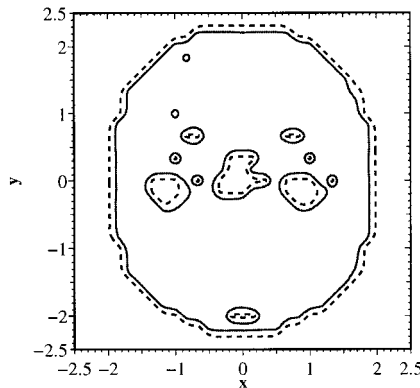


Figure 15. Contour plot of the Lyapunov exponent distribution for case G and for a  $t_{\max}$  of 20 000 s. The solid line is a contour of 0.02 and the dashed line is a 0.004 contour.

For this configuration the vortices at the ends of the line move on a circle and for all the tracer particles the Lyapunov exponent is zero. Case F is perturbed slightly resulting in case G and for this the initial configuration of vortices is  $\Gamma_1 = \Gamma_2 = \Gamma_3 = 1.0$ ;  $(x_1, y_1) = (-1, 0)$ ;  $(x_2, y_2) = (0, 0.05)$ ;  $(x_3, y_3) = (1, 0)$ . The corresponding Lyapunov exponent distribution is given in Figure 15. As seen clearly, there are a few small regular regions of motion apart from the ones near the eyes of the vortices. This is significantly different from the earlier case C, which is a slightly perturbed version of case B (vortices on an equilateral triangle). Case F is different from case B because it is unstable. This instability leads to a vortex motion that is significantly different from a circular one even when slightly perturbed.

Case H, of four vortices which move in a circle having initial configuration as  $\Gamma_1 = \Gamma_2 = \Gamma_3 = \Gamma_4 = 1.0$ ;  $(x_1, y_1) = (-1, 0)$ ;  $(x_2, y_2) = (1, 0)$ ;  $(x_3, y_3) = (0, 1)$ ;  $(x_4, y_4) = (0, -1)$  is also considered. Here too there are no regions where a positive Lyapunov exponent is seen. This case is similar to case B, wherein there is no chaotic tracer motion anywhere in the flow.

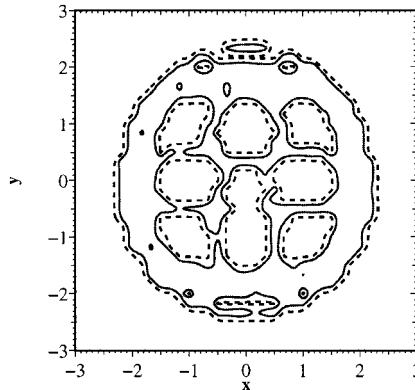


Figure 16. Contour plot of the Lyapunov exponent distribution for case I and for a  $t_{\max}$  of 20 000 s. The solid line is a contour of 0.012 and the dashed line is a 0.002 contour.

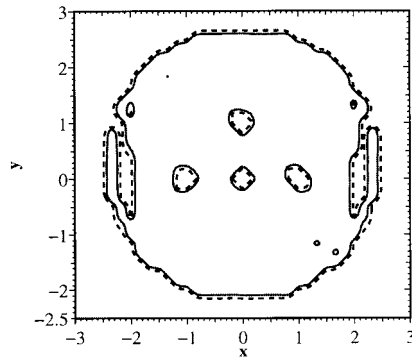


Figure 17. Contour plot of the Lyapunov exponent distribution for case J and for a  $t_{\max}$  of 20 000 s. The solid line is a contour of 0.02 and the dashed line is a 0.005 contour.

The above configuration is perturbed by a small amount resulting in case I, given as  $\Gamma_1 = \Gamma_2 = \Gamma_3 = \Gamma_4 = 1.0$ ;  $(x_1, y_1) = (-1, 0)$ ;  $(x_2, y_2) = (1, 0)$ ;  $(x_3, y_3) = (0, 0.9)$ ;  $(x_4, y_4) = (0, -1)$ . The Lyapunov exponent distribution for this is given in Figure 16. It is seen that there are large regions of regularity and small bands where there is a positive Lyapunov exponent. This is similar to that seen in Figure 12 for the corresponding three vortex problem (case C). Hence, it is seen that upon perturbing the circular orbits of the vortices, regions of chaotic tracer motion gradually appear.

Another case of four vortices is considered for which the initial vortex configuration is given by  $\Gamma_1 = \Gamma_2 = \Gamma_3 = \Gamma_4 = 1.0$ ;  $(x_1, y_1) = (-1, 0)$ ;  $(x_2, y_2) = (1, 0)$ ;  $(x_3, y_3) = (0, 1)$ ;  $(x_4, y_4) = (0, 0)$ . This is called case J and the exponent distribution for it is as given in Figure 17 and indicates that there is a small regular region near the boundary. This is similar to the earlier case E, in that the vortex configuration is greatly altered from that of its corresponding circular motion (case G).

All the above observations are made by studying the Lyapunov exponent plot at large times. For the asymmetric initial configuration of three vortices given earlier as case D, the small

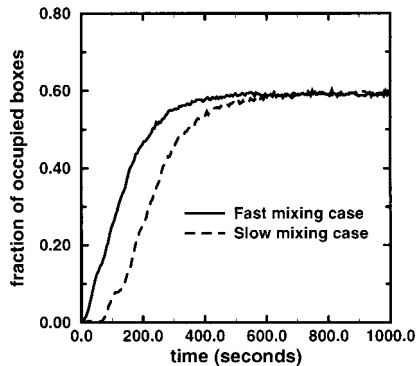


Figure 18. Mixing for fast and slow mixing regions in case D. The blobs considered have 6561 particles in them.

time exponent plot is studied and a slow mixing region is identified. This slow mixing region is centred around the point  $(0.1, 0.15)$ . A blob, initially having a dimension of  $0.1 \times 0.1$  and having 6561 particles in it, is centred at this point and the mixing of the blob is quantified as mentioned in an earlier section. Similarly a fast mixing region is identified and is centred at the point  $(0.825, 1.5)$ . A blob having the same properties is chosen for this case also. The mixing for both the fast and slow mixing regions are plotted in Figure 18. It can be seen that the blob placed initially in the fast mixing region mixes more quickly than the corresponding one in the slow mixing region. The present slow mixing is faster than that of the earlier case *viz.* Figure 8. It is to be noted that in the case of Figure 8, the slow mixing is very poor in the sense that the blob did not start stretching until after a very long time and even then the rate is much slower than the corresponding fast mixing case presented in Figure 18.

Similar to the flow in the unbounded domain, the flow of three vortices inside a cylinder was also considered and very similar results were obtained. Here too as the motion of the vortices was perturbed from circular motion, regions of chaotic tracer motion appeared and as the perturbation increased, the size of the regular regions slowly reduced just as observed above. However, these results are not presented.

In order to understand the behaviour of the Lyapunov exponent in time for the earlier mentioned integrable four-vortex motion (case J), the Lyapunov exponent for a few tracer particles is plotted with respect to time and is given in Figure 19. The plot clearly indicates that there are two types of behaviour of the Lyapunov exponents. One which rapidly converges to zero and the other which converges to a fixed positive value. All the chaotic orbits considered appear to have the same Lyapunov exponent. In order to check this for larger computational times, the computations for two of the chaotic orbits are done for a time of  $10^6$  natural time units and are plotted in Figure 20. It can be seen that they converge to one positive value.

## 8.2. Chaotic vortex motion

In this section, the results of various computations are presented for a chaotic four-vortex problem, having an initial vortex configuration given by  $\Gamma_1 = \Gamma_2 = \Gamma_3 = \Gamma_4 = 1.0$ ;  $(x_1, y_1) = (-1, 0)$ ;  $(x_2, y_2) = (1, 0)$ ;  $(x_3, y_3) = (0, 1)$ ;  $(x_4, y_4) = (0, 0.4)$ . This is called case K.

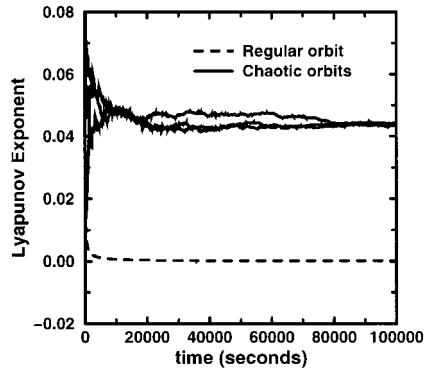


Figure 19. Plot of the Lyapunov exponent with time for the integrable vortex motion (case J).  $t_{\max}$  is 100 000 s.

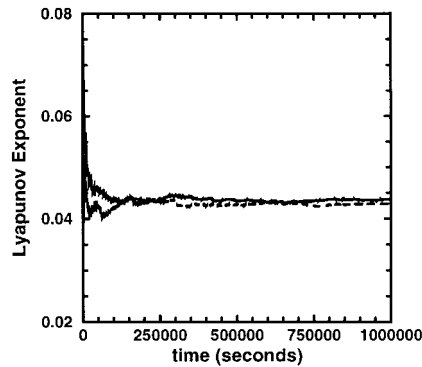


Figure 20. A plot of the Lyapunov exponent (case J) with time for two chaotic orbits.  $t_{\max}$  is 100 000 s.

In Figure 21 the behaviour of the Lyapunov exponent in time for the chaotic four-vortex motion (case K) is plotted for a few different initial conditions of tracer particles. It is seen that for one of the initial conditions the exponent rapidly converges to zero. This point is very far away from the vortices and hence its behaviour is regular. The other ones are closer to the vortices and a few appear to converge to one exponent value while a few others do not seem to do so, unlike the behaviour seen in the integrable case. In order to see if there is really a convergence to any value, the computation is again performed for a time of  $10^6$  s and as can be seen in Figure 22 the values do not converge and continue to change. This is in sharp contrast to what was seen earlier for the integrable vortex motion given in Figures 19 and 20. In order to confirm this observation, further computations are performed for a set of about 60 initial tracer locations having chaotic motion. For this set of particles, the Lyapunov exponent is computed for both the integrable vortex motion (case J) and the chaotic vortex motion (case K). The standard deviation divided by the mean of the Lyapunov exponent for various chaotic vortex motion cases and various non-chaotic vortex motion cases are computed and plotted as a function of time in Figure 23. It is seen that the value decreases and is much

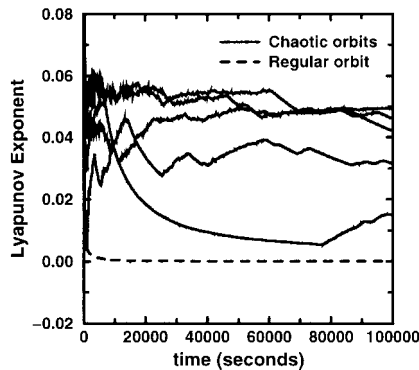


Figure 21. Plot of the Lyapunov exponent with time for the chaotic vortex motion (case K).  $t_{\max}$  is 100 000 s.

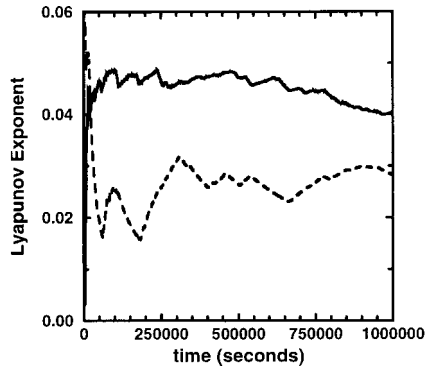


Figure 22. Plot of the Lyapunov exponent (case K) with time for two chaotic orbits.  $t_{\max}$  is 100 000 s.

less for integrable case, whereas for the chaotic case it is much higher—almost by a factor of three. However, when the exponents for the chaotic vortex motion inside a cylinder are considered such results are not seen. In Figure 24 the standard deviation divided by mean is plotted both for chaotic and regular vortex motion for a collection of about 60 particles each. It can be clearly seen that the standard deviation of the exponent is small compared with the mean, hence it appears that the Lyapunov exponents converge just as in the regular unbounded vortex motion case. For the unbounded chaotic vortex motion, computations for a smaller number of particles using smaller eps values were performed but they revealed similar results.

The Lyapunov exponent distribution for the chaotic four vortex problem (case K) is plotted in Figure 25. The regions near the eye of the vortices continue to show a regular motion. Apart from this there are several small regions where the exponents appear to be small. From the earlier plots for the convergence of the exponent it is seen that these values are not indicative of regular motion. Also from the earlier discussion of integrable vortex motion it is seen that as the initial configuration is changed from that which produces circular vortex motion, the regular regions reduce in size and ultimately such regions become negligibly small.

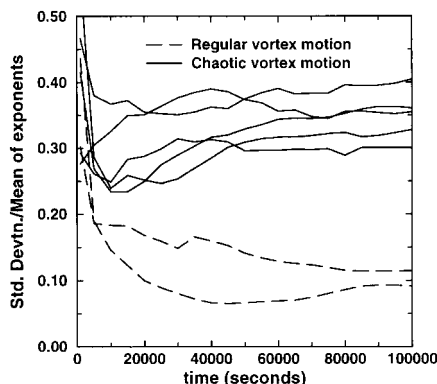


Figure 23. Plot of the standard deviation of the Lyapunov exponents divided by the mean for various tracer particles in an unbounded flow for various initial vortex configurations. The solid lines are for vortex configurations that undergo chaotic motion and the dotted lines are for regular vortex motion.

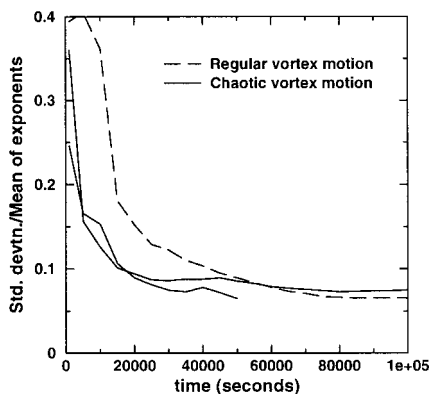


Figure 24. Plot of the standard deviation of the Lyapunov exponents divided by the mean for various tracer particles inside a circle for various initial vortex configurations. The solid lines are for vortex configurations that undergo chaotic motion and the dotted lines are for regular vortex motion.

In order to have a chaotic vortex motion the initial vortex configuration must be changed quite drastically from that which produces circular vortex motion *viz.* case H. This is seen in the configuration of vortices chosen in case K. This suggests that there should be no regular region apart from the ones near the eye of the vortices and the region far away from the vortices. This has been verified by studying the development of a blob of tracer particles in time. However, the results are not presented here. Hence, for a velocity field that displays Eulerian chaos it appears that there are no regular regions apart from the ones near the eyes of the vortices and the one that is very far away.

The small-time Lyapunov exponent distribution for the chaotic four-vortex problem is plotted for two different  $\epsilon$  values of  $10^{-7}$  and  $10^{-8}$ . Each computation is done with a different set of random angles. It is found that the plots are very similar. From the plots, two sample regions of fast and slow mixing are identified to be initially centred at  $(1.25, -0.5)$  and

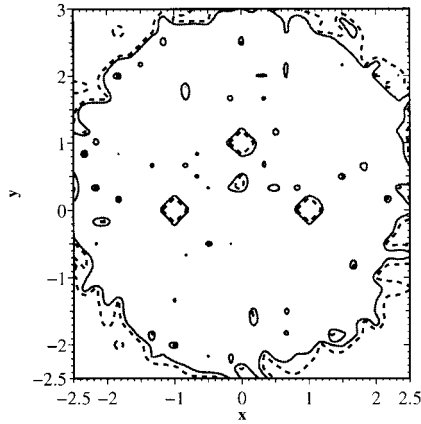


Figure 25. Contour plot of the Lyapunov exponent distribution for case K and for a  $t_{\max}$  of 20 000 s. The solid line is a 0.02 contour and the dashed line is a 0.006 contour.

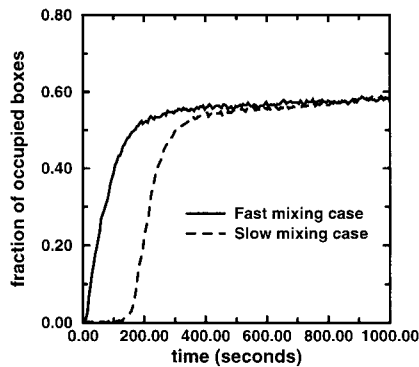


Figure 26. Mixing rates for blobs placed in fast and slow regions of mixing for the chaotic four-vortex problem (case K).

$(-0.55, 0.85)$  respectively. As is done in the previous section, the mixing of a blob in those regions is quantified by the box counting scheme. The results are presented in Figure 26. As can be seen, the blob placed in the fast mixing region starts mixing immediately and hence makes the mixing efficient there. Hence, in spite of the fact that the Lyapunov exponent does not converge in time, the method described in this paper is successful in the identification of the regions of fastest and most efficient mixing.

## 9. CONCLUSIONS

The observations made in the previous sections indicate that in the regions near the eye of the vortices and the regions far away from the vortices, the tracer particles exhibit regular, non-chaotic motion irrespective of the nature of the vortex motion (regular or chaotic). This result

is consistent with that obtained by Babiano *et al.* [6]. However, the method described in this paper has identified other regions of regular motion. It is also observed that only significantly large changes of the initial configuration of vortices from the one which produces a circular vortex motion leads to the creation of large regions of chaotic tracer motion. Hence, it can be stated that there is a strong connection between the vortex motion and the regions of regularity that are not near the eye of the vortices.

It has also been shown in this paper that from the knowledge of the small-time Lyapunov exponent distribution, the regions of most efficient mixing for a given initial configuration of vortices can be identified. This technique is also shown to be accurate and much more efficient than the traditional box counting scheme.

From the computations presented in this paper it is seen that for a chaotic four-vortex motion in the unbounded domain, the Lagrangian Lyapunov exponent does not converge properly. For integrable vortex motion, the exponent is shown to converge. It has also been shown that for chaotic vortex motion inside a cylinder, the Lyapunov exponent converges. Hence, care must be taken while interpreting long-time Lyapunov exponent values for unbounded chaotic vortex motion cases. At this juncture it is not possible to say if the non-convergence is due to numerical error or due to a more fundamental problem.

The procedure used to identify the regions of highest mixing is general and can also be applied to other flows (including three-dimensional flows) so long as the trajectory of the particle can be computed. Hence, the regions of most efficient mixing can be identified by studying the distribution of the largest Lagrangian Lyapunov exponent for large and small times. Thus, the present method of identification of regions of fast mixing appears to be promising.

#### ACKNOWLEDGEMENTS

Most of the computations were performed at the computational facility of the Department of Aerospace Engineering, IIT Madras. The authors wish to thank Dr P. Sriram and Dr M. Ramakrishna, Associate Professors, Department of Aerospace Engineering, IIT Madras, for their help and guidance. They also wish to thank Dr Neelima Gupte, Assistant Professor, Department of Physics, IIT Madras for her useful suggestions; express their gratitude to S. Shashidhar, MS Scholar, Department of Aerospace Engineering, IIT Madras (presently with Flow Consultants, Pune, India) for his help in the preparation of this article.

#### REFERENCES

1. Ottino JM. *The Kinematics of Mixing: Stretching, Chaos, and Transport*. Cambridge University Press: Cambridge, 1989.
2. Novikov EA. Dynamics and statistics of a system of vortices. *Soviet Physics JETP* 1984; **41**:937.
3. Aref H. Motion of three vortices. *Physics of Fluids* 1979; **22**(3):393.
4. Aref H, Pomphrey N. Integrable and chaotic motions of four vortices. *Physics Letters* 1980; **78A**(4):297.
5. Aref H, Pomphrey N. Integrable and chaotic motions of four vortices I—the case of identical vortices. *Proceedings of the Royal Society London Series A* 1982; **380**:359.
6. Babiano A, Bofetta G, Provenzale A, Vulpiani A. Chaotic advection in point vortex models and two-dimensional turbulence. *Physics of Fluids* 1994; **6**(7):2465.
7. Aref H. Stirring by chaotic advection. *Journal of Fluid Mechanics* 1984; **143**:1.
8. Franjione JG, Ottino JM. Feasibility of numerical tracking of material lines and surfaces in chaotic flows. *Physics of Fluids* 1987; **30**:3641.
9. Aref H. Integrable, chaotic, and turbulent vortex motion in two dimensional flows. *Annual Review in Fluid Mechanics* 1983; **15**:345.

10. Prabhu R. Chaos and mixing in vortex dominated flows. *Bachelor of Technology Thesis*, Indian Institute of Technology Madras, 1997.
11. Press WH, Teukolsky SA, Vetterling WT, Flannery BP. *Numerical Recipes in 'C'*. Cambridge University Press: Cambridge, 1992.
12. Peitgens HO, Jurgens H, Saupe D. *Chaos and Fractals, New Frontiers of Science*. Springer: New York, 1992.